

# **The influence of grain boundary and hydrogen on the indentation of bi-crystal nickel**

**Kaiyu Zhang<sup>1</sup>, Yuanyuan Zheng<sup>2</sup>, Chengshuang Zhou<sup>2</sup>, Jinyang Zheng<sup>4</sup> and Lin Zhang<sup>5</sup>**

**<sup>1</sup> Institute of Material Forming and Control Engineering, Zhejiang University of Technology,  
Hangzhou 310014, China, 1120846730@qq.com**

**<sup>2</sup> School of Mechanical and Energy Engineering, Zhejiang University of Science and Technology,  
Hangzhou 310023, China, 954261238@qq.com**

**<sup>3</sup> Institute of Material Forming and Control Engineering, Zhejiang University of Technology,  
Hangzhou 310014, China, zhousc@zjut.edu.cn**

**<sup>4</sup> Institute of Chemical Machinery Engineering, Zhejiang University, Hangzhou 310027, China,  
jyzh@zju.edu.cn**

**<sup>5</sup> Institute of Material Forming and Control Engineering, Zhejiang University of Technology,  
Hangzhou 310014, China, zhlin@zjut.edu.cn**

## **ABSTRACT**

Three different types of symmetrical tilt grain boundaries,  $\Sigma 3$ ,  $\Sigma 11$ , and  $\Sigma 27$ , were constructed to study the dislocation behavior under the indentation on bi-crystal nickel. After hydrogen charging, the number of hydrogen atoms in the  $\Sigma 3$  sample is the smallest and gradually increases in  $\Sigma 11$  and  $\Sigma 27$  samples. The force-displacement curve of indentation shows that the deformation resistance of the  $\Sigma 3$  sample is significantly higher than that of  $\Sigma 11$  and  $\Sigma 27$  samples. With the presence of grain boundaries, the deformation resistance of  $\Sigma 11$  and  $\Sigma 27$  samples is significantly improved, while the deformation resistance of the  $\Sigma 3$  sample is weakened. The indentation depth during the formation of dislocations in single crystals is significantly greater than that of bi-crystals. Grain boundaries slow down the dislocation propagation speed. Compared with the bi-crystals without hydrogen, the presence of hydrogen reduces the deformation resistance and accelerates the dislocation propagation.

## **1. Introduction**

For decades, hydrogen has been regarded as a major factor in reducing the mechanical properties of metallic materials[1–4]. During the production and service of the materials, hydrogen atoms from different sources can enter into the matrix. Hydrogen can be rapidly diffused and trapped through material internal defects such as vacancies, dislocations, grain boundaries, etc. Although a great deal of research has been done, the effect of hydrogen on the mechanical properties of metals remains unclear.[5–9]

Nowadays, molecular simulation(MD) is widely used to explain the mechanism that cannot be achieved experimentally. A lot of studies on the relationship between hydrogen and mechanical properties have been done[10–14]. Zheng et al.[15] studied the coupling effect of grain boundary and hydrogen segregation on dislocation nucleation in bi-crystal nickel. The result shows that hydrogen promotes dislocation nucleation and emission in the high energy grain boundary and decreases the yield strength, whereas the low energy grain boundary is the opposite. Li et al.[16] studied the hydrogen-modified interaction between lattice dislocation and grain boundaries, and found that the presence of hydrogen tends to enhance dislocation absorbed by the grain boundary. Song et al.[17] found that hydrogen atoms have no influence on the primary dislocation (or twin) nucleation mechanism, but rather influence their multiplication process. And the degree of hydrogen embrittlement is dependent on the misorientation angle, but it is almost independent of the grain size.

Most of these studies investigated the effect of hydrogen under tensile conditions. In this research, we focused on the influence of grain boundary and hydrogen under indentation, and the effect on dislocation formation and propagation was discussed.

## **2. Simulation details**

All the atomistic simulations were performed via LAMMPS (Large-scale Atomic/Molecular Massively Parallel Simulator)[18], and embedded-atom method potential[19] was used to describe the interaction between Ni and H. Three different types of symmetrical tilt grain boundaries (STGB) were constructed, which were respectively referred to as  $\Sigma 3$ ,  $\Sigma 11$ , and  $\Sigma 27$  samples. The x-, y- and z-axis orientations were shown in Table 1, and the dimensions of the simulation cell were about 300, 300, and 30 Å (Figure 1), containing about 240,000 atoms. The time step in all the MD simulations was set to be 1 fs. The conjugate-gradient algorithm was used to minimize the energy of the structures, and then samples relaxed at 300 K for 20 ps to achieve the equilibrium state. Grand Canonical Monte Carlo(GCMC) was used for hydrogen charging with a chemical potential for -2.4 eV.

During indentation, samples were under the NVE ensemble. The boundary of the simulation cell was periodic along x- and z-direction, and fixed along the y-direction. The bottom three layers of atoms were fixed to prevent samples from moving, and the next four layers of atoms were kept at a constant temperature of 300 K with the Nose-Hoover thermostat as thermostat atoms. Other atoms were set as Newtonian atoms, and their motion was described by the Newton equation. The cylindrical rigid indenter with a radius of 50 Å was loaded along the y- axis, and the speed of indentation was 10m/s. The atomic

structure of samples was analyzed by OVITO software.

Table 1. Grain orientations for  $\Sigma 3$ ,  $\Sigma 11$  and  $\Sigma 27$  samples.

Types of STGB	Grain orientations					
	$x_1$	$y_1$	$z_1$	$x_2$	$y_2$	$z_2$
$\Sigma 3$	1 1 2	$\bar{1}$ $\bar{1}$ 1	1 $\bar{1}$ 0	1 1 $\bar{2}$	1 1 1	1 $\bar{1}$ 0
$\Sigma 11$	3 3 2	$\bar{1}$ $\bar{1}$ 3	1 $\bar{1}$ 0	3 3 $\bar{2}$	1 1 3	1 $\bar{1}$ 0
$\Sigma 27$	5 5 2	$\bar{1}$ $\bar{1}$ 5	1 $\bar{1}$ 0	5 5 $\bar{2}$	1 1 5	1 $\bar{1}$ 0

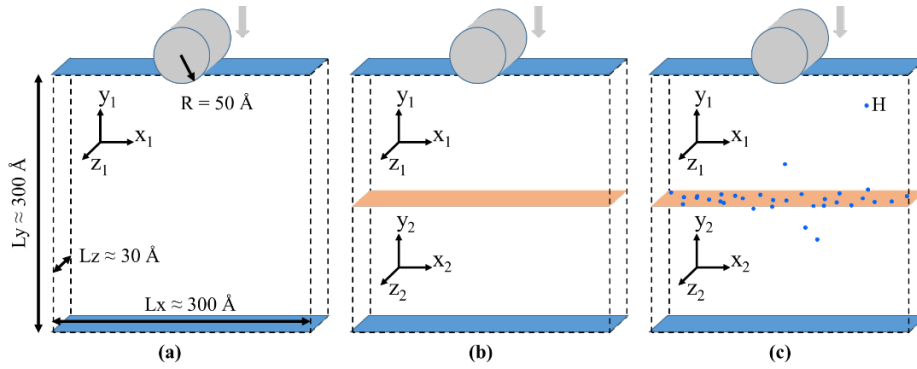


Figure 1. Schematic of the indentation simulation box. (a) Single crystal samples; (b) Bi-crystal samples without hydrogen atoms; (c) Bi-crystal samples with hydrogen atoms.

### 3. Results

#### 3.1 Hydrogen distribution after hydrogen charging

The distribution of hydrogen atoms in different bi-crystal after hydrogen charging is shown in Figure 2(a, b and c). The number of hydrogen atoms is 17, 122 and 336 respectively. The H atoms in the  $\Sigma 3$  sample are fewest and uniformly distributed. Different from the  $\Sigma 3$  sample, the H atoms in  $\Sigma 11$  and  $\Sigma 27$  samples are mainly distributed at the grain boundary. As shown in Figure 2d, the number of H atoms and the grain boundary energy in  $\Sigma 3$ ,  $\Sigma 11$ , and  $\Sigma 27$  samples have the same trend. Grain boundary has a great influence on the quantity and distribution of hydrogen atoms after hydrogen charging.

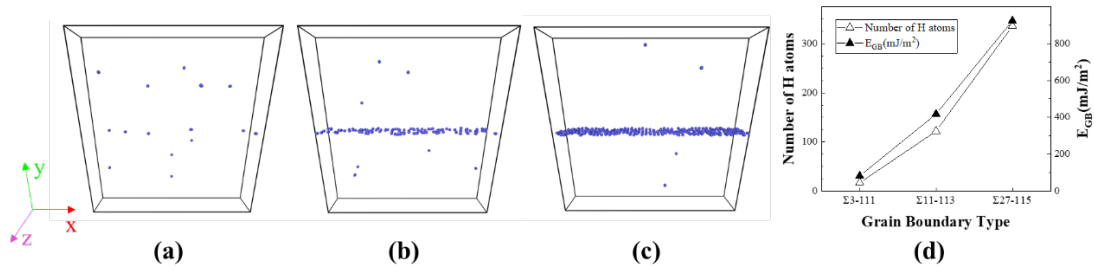


Figure 2. Hydrogen distribution after hydrogen charging. (a)  $\Sigma 3$  sample; (b)  $\Sigma 11$  sample; (c)  $\Sigma 27$  sample; (d) Number of H atoms and GB energy for different samples.

### 3.2 Effect of grain boundary on indentation

The force-distance curve for  $\Sigma 3$ ,  $\Sigma 11$ , and  $\Sigma 27$  single crystal and bi-crystal samples is shown in Figure 3. Compared with the curve of three single crystal samples, the force on  $\Sigma 3$  sample is much higher than that on  $\Sigma 11$  and  $\Sigma 27$  samples. For the bi-crystal samples, the force on  $\Sigma 3$  sample is also highest and that on  $\Sigma 27$  is the smallest. Considering the presence of grain boundaries, there are two different effects. The force on  $\Sigma 3$  sample is decreased with the influence of grain boundary, while the force on  $\Sigma 11$  and  $\Sigma 27$  samples is increased.

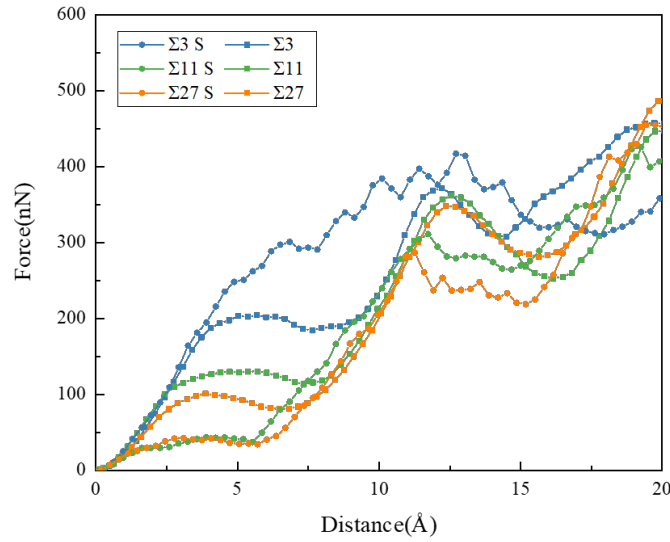


Figure 3. The force-distance curve for  $\Sigma 3$ ,  $\Sigma 11$ , and  $\Sigma 27$  single crystal and bi-crystal samples.

Dislocation Analysis(DXA) was used to analyze the presence and movement of dislocation at different indentation distances. The DXA results are shown in Figure 4, and snapshots at different indentation distances represent dislocation formation, dislocation slip, dislocation reaching the grain boundary, and dislocation crossing the grain boundary, respectively. The distance of each snapshot is indicated above the snapshot. The indentation distance of single crystal samples at which the dislocation

is formed is much greater than that of bi-crystal samples. The time of dislocation propagation to the grain boundary is also much shorter in single crystal samples than in bi-crystal samples. Those results mean that grain boundaries can prevent the formation and propagation of dislocation.




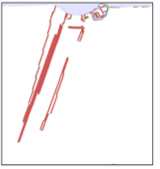
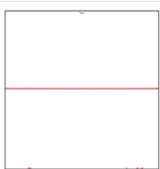
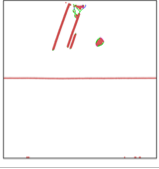
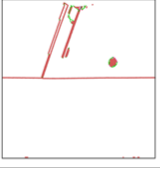
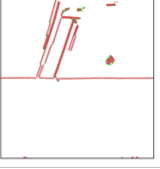

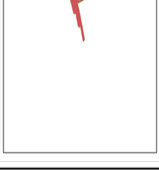


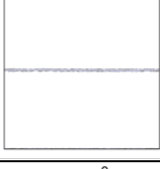
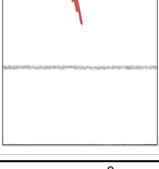
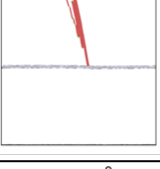
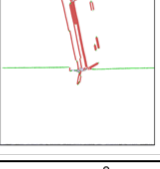
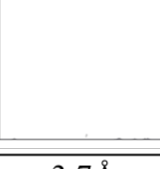

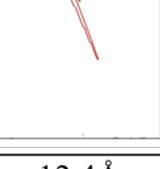
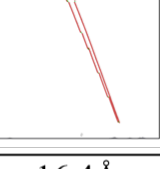
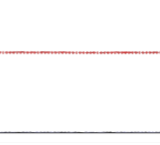
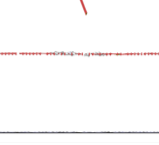
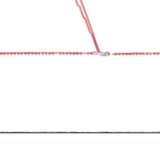
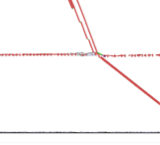
	Dislocation formation	2Å before dislocation reaching GB	Dislocation reaching GB	4Å after dislocation reaching GB
<b><math>\Sigma 3</math> S</b>	9.5Å 	10.6Å 	12.6Å 	16.6Å 
<b><math>\Sigma 3</math></b>	2.4Å 	9.7Å 	11.7Å 	15.7Å 
<b><math>\Sigma 11</math> S</b>	7.3Å 	9.8Å 	11.8Å 	15.8Å 
<b><math>\Sigma 11</math></b>	2.7Å 	10.4Å 	12.4Å 	16.4Å 
<b><math>\Sigma 27</math> S</b>	6.5Å 	10.8Å 	12.8Å 	16.8Å 
<b><math>\Sigma 27</math></b>	3.7Å 	10.4Å 	12.4Å 	16.4Å 

Figure 4. Snapshots of DXA at different indentation distance for  $\Sigma 3$ ,  $\Sigma 11$ , and  $\Sigma 27$  single crystal and bi-crystal samples.

### 3.3 Effect of hydrogen on indentation

The force-distance curves of the  $\Sigma 3$ ,  $\Sigma 11$ , and  $\Sigma 27$  samples with and without hydrogen atoms are shown in Figure 5. The variation trend of the curves is almost the same except that the samples with hydrogen atoms have a period of decrease before the distance of 10 Å. The decline of the force is the most obvious in  $\Sigma 27$  sample, and the smallest in  $\Sigma 3$  sample. Therefore, hydrogen atoms can weaken the effect of grain boundary, especially in  $\Sigma 27$  sample.

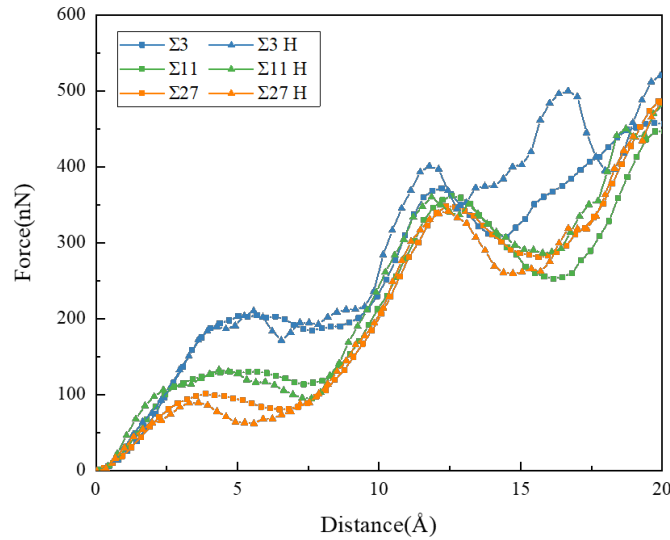


Figure 5. The force-distance curve for  $\Sigma 3$ ,  $\Sigma 11$ , and  $\Sigma 27$  bi-crystal samples with and without hydrogen atoms.

DXA is also used to analyze the atom structures of the samples with and without hydrogen atoms, as shown in Figure 6. Hydrogen atoms put off the formation of dislocation in  $\Sigma 3$  and  $\Sigma 27$  samples, but facilitate the formation of dislocation in  $\Sigma 11$  sample. Compared with the time of samples with or without hydrogen atoms for dislocation propagation to the grain boundary, hydrogen atoms accelerate the movement of dislocation.

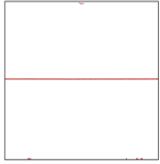

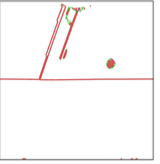
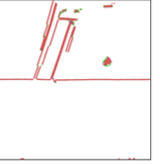

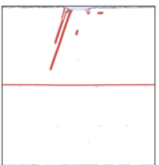
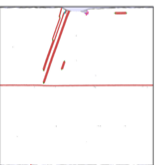
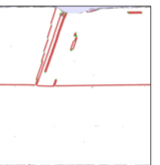
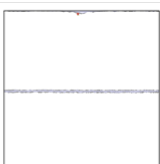
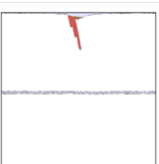
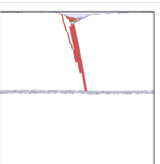
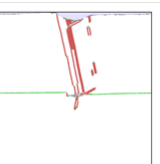
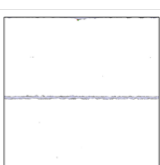
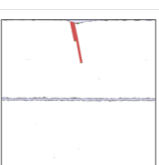
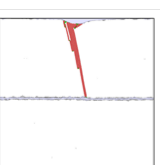
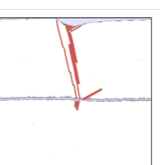
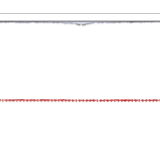
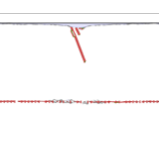
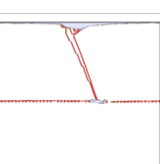
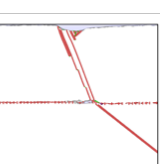
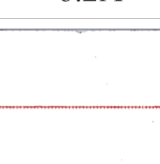
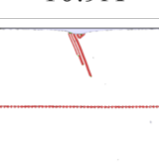
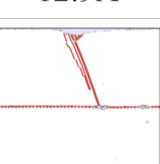
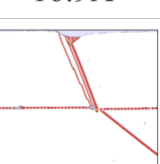
	Dislocation formation	2Å before dislocation reaching GB	Dislocation reaching GB	4Å after dislocation reaching GB
$\Sigma 3$	2.4Å 	9.7Å 	11.7Å 	15.7Å 
$\Sigma 3$ H	3.3Å 	6.7Å 	8.7Å 	12.7Å 
$\Sigma 11$	2.7Å 	10.4Å 	12.4Å 	16.4Å 
$\Sigma 11$ H	1.9Å 	8.8Å 	10.8Å 	14.8Å 
$\Sigma 27$	3.7Å 	10.4Å 	12.4Å 	16.4Å 
$\Sigma 27$ H	6.2Å 	10.9Å 	12.9Å 	16.9Å 

Figure 6. Snapshots of DXA at different indentation distance for  $\Sigma 3$ ,  $\Sigma 11$ , and  $\Sigma 27$  bi-crystal samples with and without hydrogen atoms.

#### 4. Discussion

The previous study has shown that hydrogen accommodation within the grain boundaries strongly depends on the local coordination of the available interstitial sites[20]. As shown in Figure 7, the grain

boundary structures of  $\Sigma 3$ ,  $\Sigma 11$  and  $\Sigma 27$  samples can be divided into more smaller structural units [21].  $\Sigma 3$  and  $\Sigma 11$  grain boundaries are constituted by D and C structural units respectively, while  $\Sigma 27$  grain boundary is constituted by A, B and C structural units. The D structural unit has less free volume than other structural units and is closely related to the Shockley partial dislocation. Therefore, the open grain boundary structures such as  $\Sigma 27$  have larger interstitial sites than the bulk phase so that hydrogen is more likely to converge at the grain boundary and its solubility is increased. For the  $\Sigma 3$  sample, the grain boundary energy is much lower and hydrogen segregation is weak, thus there will be more H atoms are present in the bulk.

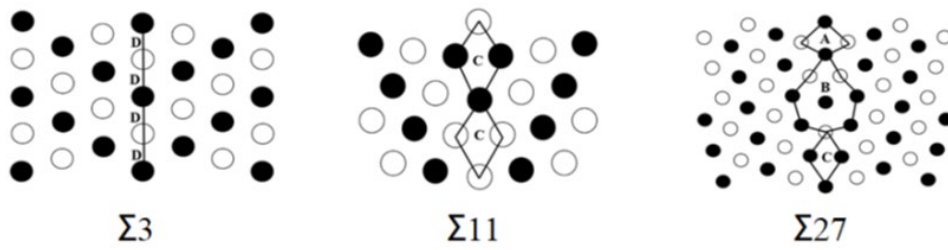


Figure 7. Structure of  $\Sigma 3$ ,  $\Sigma 11$  and  $\Sigma 27$  grain boundary.

For single crystal samples,  $\Sigma 3$ ,  $\Sigma 11$  and  $\Sigma 27$  samples have different orientations along the direction of indentation, and therefore affected by anisotropy, the deformation resistance is different. The stress-strain curve of the single crystal specimen under tension is shown in Figure 8. It shows that  $\Sigma 3$  samples with the  $\langle 111 \rangle$  direction along y-axis have higher deformation resistance than  $\Sigma 11$  and  $\Sigma 27$  samples, which are consistent with the curve in Figure 3.

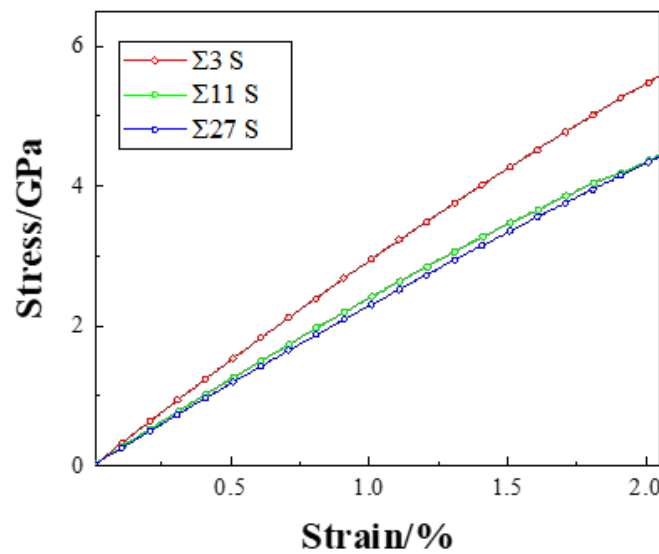


Figure 8. Stress-strain curve of single crystal specimen under tension.

The snapshots of dislocations crossing grain boundary colored with atomic strain are shown in

Figure 9. Generally, grain boundaries have a hardening effect on indentation[22], and grain boundaries in bi-crystal can be thought of as barriers to the movement of atoms under indentation, and that is why the force on  $\Sigma 11$  and  $\Sigma 27$  bi-crystal samples increases. But for  $\Sigma 3$  bi-crystal samples, there are more directions for dislocations slip and the dislocation is absorbed by the grain boundary, as a result, the force on samples decreases compared to the single crystal sample. For the samples with hydrogen atoms, the free volume of grain boundaries is occupied with hydrogen atoms. When the dislocation achieves the grain boundaries, the reaction between dislocation and grain boundaries is inhibited, so dislocation crosses the grain boundary rapidly.

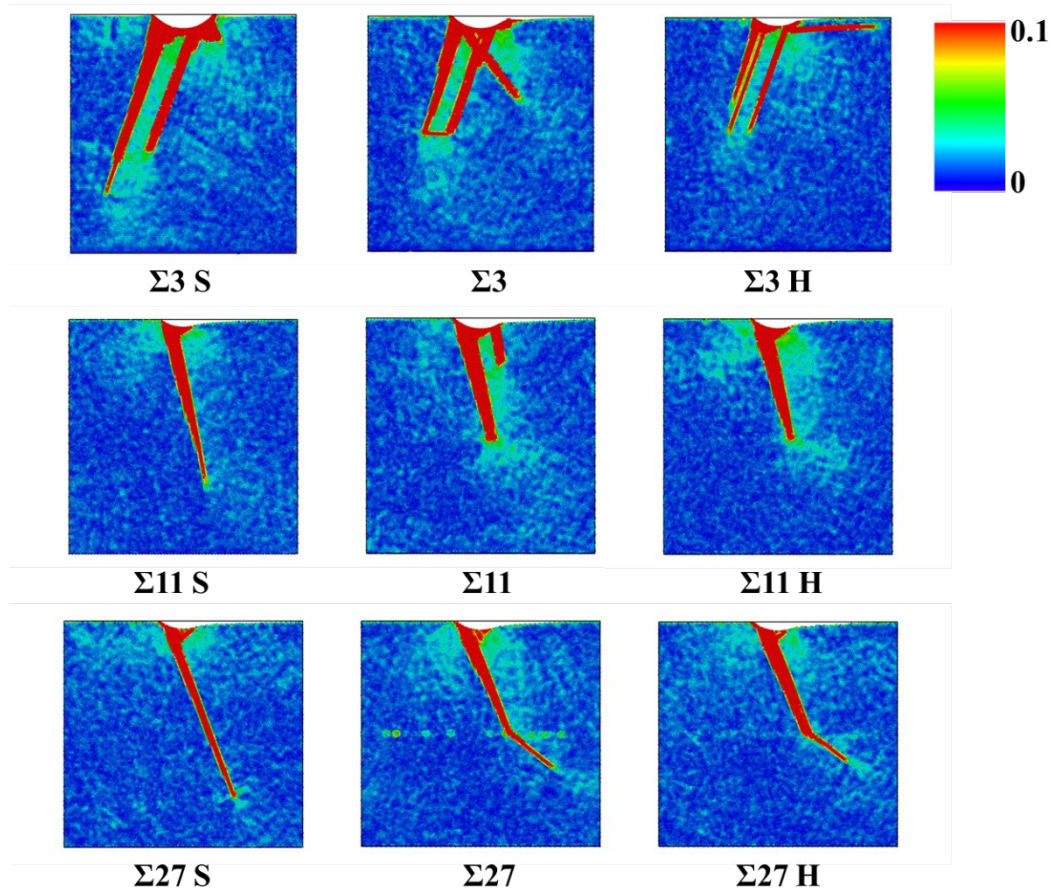


Figure 9. Snapshots of dislocations crossing grain boundary colored with atomic strain.

## 5. Conclusions

In this work, three different types of symmetrical tilt grain boundary were constructed to study the influence of grain boundary and hydrogen on the indentation of Nickel. The main findings are summarized as follows:

- (1) The number of hydrogen atoms after hydrogen charging is strongly related to the grain boundary structure.

- (2) Grain boundaries act as the barrier to the movement of atoms, improve the deformation resistance of the samples and accelerate the formation of dislocation.
- (3) The free volume in grain boundary is occupied by hydrogen atoms after hydrogen charging. The presence of hydrogen reduces the deformation resistance and accelerates the dislocation propagation.

### Acknowledgments

This research was supported by the National Key Research and Development Program of China (2019YFB1505302), the National Natural Science Foundation of China (51971204), and the Zhejiang Provincial Natural Science Foundation of China (LY19E010006, LY21E010005).

### References

- [1] Robertson IM, Sofronis P, Nagao A, Martin ML, Wang S, Gross DW, et al. Hydrogen Embrittlement Understood. *Metall Mater Trans B* 2015;46:1085–103.  
<https://doi.org/10.1007/s11663-015-0325-y>.
- [2] Martin ML, Somerday BP, Ritchie RO, Sofronis P, Robertson IM. Hydrogen-induced intergranular failure in nickel revisited. *Acta Mater* 2012;60:2739–45.  
<https://doi.org/https://doi.org/10.1016/j.actamat.2012.01.040>.
- [3] Xie W, Liu X, Chen W, Zhang H. Hydrogen hardening effect in heavily deformed single crystal  $\alpha$ -Fe. *Comput Mater Sci* 2011;50:3397–402.  
<https://doi.org/https://doi.org/10.1016/j.commatsci.2011.06.036>.
- [4] Siddiqui RA, Abdul-Wahab SA, Bakheit CS. Investigating the variation in the properties of hydrogenated 0.31% carbon steel. *Mater Des* 2008;29:922–7.  
<https://doi.org/https://doi.org/10.1016/j.matdes.2007.04.007>.
- [5] Lynch SP. Interpreting hydrogen-induced fracture surfaces in terms of deformation processes: A new approach. *Scr Mater* 2011;65:851–4.  
<https://doi.org/https://doi.org/10.1016/j.scriptamat.2011.06.016>.
- [6] Villalobos JC, Serna SA, Campillo B, López-Martínez E. Evaluation of mechanical properties of an experimental microalloyed steel subjected to tempering heat treatment and its effect on hydrogen embrittlement. *Int J Hydrogen Energy* 2017;42:689–98.  
<https://doi.org/https://doi.org/10.1016/j.ijhydene.2016.10.103>.
- [7] Olden V, Alvaro A, Akselsen OM. Hydrogen diffusion and hydrogen influenced critical stress

- intensity in an API X70 pipeline steel welded joint – Experiments and FE simulations. *Int J Hydrogen Energy* 2012;37:11474–86.  
<https://doi.org/https://doi.org/10.1016/j.ijhydene.2012.05.005>.
- [8] da Silva BRS, Salvio F, Santos DS dos. Hydrogen induced stress cracking in UNS S32750 super duplex stainless steel tube weld joint. *Int J Hydrogen Energy* 2015;40:17091–101.  
<https://doi.org/https://doi.org/10.1016/j.ijhydene.2015.08.028>.
- [9] Robertson IM. The effect of hydrogen on dislocation dynamics. *Eng Fract Mech* 2001;68:671–92. [https://doi.org/https://doi.org/10.1016/S0013-7944\(01\)00011-X](https://doi.org/https://doi.org/10.1016/S0013-7944(01)00011-X).
- [10] Li J, Lu C, Pei L, Zhang C, Tieu K. Influence of solute hydrogen on the interaction of screw dislocations with vicinal twin boundaries in nickel. *Scr Mater* 2019;173:115–9.  
<https://doi.org/https://doi.org/10.1016/j.scriptamat.2019.08.010>.
- [11] Zhou X-Y, Zhu J-H, Wu H-H. Molecular dynamics studies of the grain-size dependent hydrogen diffusion coefficient of nanograined Fe. *Int J Hydrogen Energy* 2021;46:5842–51.  
<https://doi.org/https://doi.org/10.1016/j.ijhydene.2020.11.131>.
- [12] Li J, Lu C, Pei L, Zhang C, Wang R, Tieu K. Atomistic simulations of hydrogen effects on tensile deformation behaviour of [0 0 1] twist grain boundaries in nickel. *Comput Mater Sci* 2019;159:12–23. <https://doi.org/https://doi.org/10.1016/j.commatsci.2018.11.048>.
- [13] Wan L, Geng WT, Ishii A, Du J-P, Mei Q, Ishikawa N, et al. Hydrogen embrittlement controlled by reaction of dislocation with grain boundary in alpha-iron. *Int J Plast* 2019;112:206–19. <https://doi.org/https://doi.org/10.1016/j.ijplas.2018.08.013>.
- [14] Xie D-G, Wan L, Shan Z-W. Hydrogen enhanced cracking via dynamic formation of grain boundary inside aluminium crystal. *Corros Sci* 2021;183:109307.  
<https://doi.org/https://doi.org/10.1016/j.corsci.2021.109307>.
- [15] Zheng Y, Yu P, Zhang K, Wen M, Zheng J, Zhou C, et al. Coupling effect of grain boundary and hydrogen segregation on dislocation nucleation in bi-crystal nickel. *Int J Hydrogen Energy* 2020;45:20021–31. <https://doi.org/https://doi.org/10.1016/j.ijhydene.2020.04.291>.
- [16] Li J, Lu C, Pei L, Zhang C, Wang R. Hydrogen-modified interaction between lattice dislocations and grain boundaries by atomistic modelling. *Int J Hydrogen Energy* 2020;45:9174–87. <https://doi.org/https://doi.org/10.1016/j.ijhydene.2020.01.103>.
- [17] Song HY, Li CF, Geng SF, An MR, Xiao MX, Wang L. Atomistic simulations of effect of

- hydrogen atoms on mechanical behaviour of an  $\alpha$ -Fe with symmetric tilt grain boundaries. Phys Lett A 2018;382:2464–9. <https://doi.org/https://doi.org/10.1016/j.physleta.2018.06.005>.
- [18] Plimpton S. Fast Parallel Algorithms for Short-Range Molecular Dynamics. J Comput Phys 1995;117:1–19. <https://doi.org/10.1006/jcph.1995.1039>.
- [19] Angelo JE, Moody NR, Baskes MI. Trapping of hydrogen to lattice defects in nickel. Model Simul Mater Sci Eng 1995;3:289–307. <https://doi.org/10.1088/0965-0393/3/3/001>.
- [20] Du YA, Ismer L, Rogal J, Hickel T, Neugebauer J, Drautz R. First-principles study on the interaction of H interstitials with grain boundaries in  $\alpha$ - and  $\gamma$ -Fe. Phys Rev B 2011;84:144121. <https://doi.org/10.1103/PhysRevB.84.144121>.
- [21] J., D., Rittner, D., N., Seidman.  $\langle 110 \rangle$  symmetric tilt grain-boundary structures in fcc metals with low stacking-fault energies. Phys Rev B 1996;54:6999–7015.
- [22] Lu S, Zhang B, Li X, Zhao J, Zaiser M, Fan H, et al. Grain boundary effect on nanoindentation: A multiscale discrete dislocation dynamics model. J Mech Phys Solids 2019;126:117–35. <https://doi.org/https://doi.org/10.1016/j.jmps.2019.02.003>.